1997 ASME Fluids Engineering Division Summer Meeting
FEDSM'97
June 22 - 26, 1997

FEDSM97-3073

DROPLET IMPACT ONTO ARBITRARY SURFACE GEOMETRIES

Markus Bussmann, Sanjeev Chandra & Javad Mostaghimi
Department of Mechanical & Industrial Engineering
University of Toronto
5 King's College Road, Toronto, Canada M5S 3G8

ABSTRACT

The normal impact of a liquid droplet onto a flat surface is a two-dimensional phenomenon, and has been extensively studied. But what of the impact of a droplet onto an inclined surface, or any other more complicated surface geometry? We present both numerical and experimental views of the impact of a water droplet onto an incline and onto an edge. The numerical model is an improved three-dimensionalization of RIPPLE (LA-12007-MS), a VOF-based finite-volume code. Model simulations are compared with sequences of photographs of the impact of a water droplet. We discuss the model, in particular improvements to the original RIPPLE, and the implementation of boundary conditions at the contact line between liquid and solid. We also present a quantitative comparison of the model and experiment; agreement is good.

INTRODUCTION

The impact of a single droplet onto a solid surface is a fundamental phenomenon in a variety of spray applications (e.g. spray cooling, thermal spraying, spray forming). A common characteristic of these processes is the dramatic deformation of individual droplets as they strike upon solid surfaces. Almost all previous studies of droplet impact have considered the two-dimensional scenario of the normal impact of a droplet onto a flat surface. Many aspects of such an impact have been extensively studied: the effect of the initial Reynolds and Weber numbers on the spread and possible recoil of the droplet (Chandra and Avedisian, 1991; Fukai et al., 1995; Pasandideh-Fard et al., 1996); heat transfer within the droplet and to or from the solid surface (Zhao et al., 1996a and 1996b); solidification of molten droplets impacting a cold surface (Trapaga et al., 1992).

On the other hand, little is known of droplet impact even onto an inclined surface, much less any arbitrary surface geometry. For example, how do fluid droplets impact onto an edge, or into a pore, or onto a curved surface?

We present numerical and experimental views of the impact of a water droplet onto a 45° incline and onto a sharp edge. Agreement between experiment and model is good. We also describe the model, and the implementation of boundary conditions.

EXPERIMENTAL TECHNIQUE

The technique used to photograph droplet impact is presented in detail by Chandra and Avedisian (1991). In summary, droplets are generated by pumping water through a hypodermic needle and allowing them to detach under their own weight. Droplets are uniformly 2 mm in diameter. A polished stainless steel surface is placed 50 mm below the needle tip, so that droplet velocity at impact is 1 m/s. A single 35 mm photograph is taken of any one instant of an impact, as determined by a set time delay between droplet release and flash illumination. The photographs of a droplet at any one instant are sufficiently repeatable from one droplet to the next that a complete impact may be reconstructed from individual photographs of different droplets.

For the impact of a droplet onto a 45° incline, we measured liquid-solid contact angles and contact diameters from enlarged photographs. Details of the measurement technique have been presented by Pasandideh-Fard et al. (1996). Most contact angles were readily measured to within ± 3°. However, as we describe later, as the droplet slides down the incline, a thin layer of fluid is dragged behind. The receding contact angle decreases to approximately 20°, and the corresponding error becomes proportionately larger.

NUMERICAL METHOD

Our numerical model is a 3D implementation of RIPPLE (Kothe et al., 1991), originally a 2D Eulerian fixed-grid fluid

dynamics code written specifically for free surface flows with surface tension. RIPPLE was chosen as the basis of our model primarily for two reasons: (i) a novel approach to modeling surface tension, which could readily be extended to three dimensions; (ii) the capability to model gross fluid deformation, including breakup. In the process of three-dimensionalizing the original RIPPLE, we incorporated improvements to the model, particularly to the algorithms which track the free surface and evaluate surface tension.

Equations of conservation of mass and momentum govern the flow of fluid within a droplet:

$$\vec{\nabla} \cdot \vec{V} = 0 \tag{1}$$

$$\frac{\partial \vec{V}}{\partial t} + \vec{\nabla} \cdot (\vec{V}\vec{V}) = -\frac{1}{\rho}\vec{\nabla} p + \upsilon \nabla^2 \vec{V} + \frac{1}{\rho}\vec{F}_b \tag{2}$$

$\vec{V}$ is the velocity vector, p the pressure, ρ the density, υ the kinematic viscosity and $\vec{F}_b$ represents any body forces acting on the fluid. Boundary conditions imposed on the equations include the standard no-slip condition for fluid in contact with a solid surface, the imposition of a contact angle at the contact line between droplet and substrate, and specification of the surface tension-induced pressure jump p_s across the free surface, according to Laplace's equation:

$$p_s = \sigma\kappa \tag{3}$$

σ represents the surface tension of the fluid and κ the local curvature of the free surface.

The equations are discretized in a typical control volume formulation. Convective, viscous and surface tension effects are evaluated explicitly, thus limiting the timestep by which the solution may be advanced. Pressure is evaluated implicitly at the end of each timestep to enforce mass conservation. Details of the numerical discretization are similar to those presented in the original documentation for RIPPLE (Kothe et al., 1991).

The free surface is represented by a so-called Volume of Fluid (VOF) function F, defined as equal to one within the fluid and zero without. In discretized form, F represents the fraction of a control volume filled with fluid: one for a full control volume, zero for an empty control volume, and $0 < F < 1$ for a control volume containing a portion of the free surface. Within this framework, the free surface is propagated according to:

$$\frac{\partial F}{\partial t} + (\vec{V} \cdot \vec{\nabla})F = 0 \tag{4}$$

In the original RIPPLE, equation (4) was discretized according to the method of Hirt and Nichols (1981). We have replaced this treatment in our model with a more accurate scheme devised by Youngs (1984). Especially in 3D, accurate discretizations are vital to offset the practical limits placed on grid refinement. In Youngs' approach, the VOF distribution is used to construct a geometric plane in each surface control volume, corresponding to the local value of F and to the direction of the normal to the interface. At each timestep, the position of an interface plane and the velocities at the control volume faces allow one to determine fluxes of F during the timestep, and thereby the values of F at the new time level.

The second significant modification to the original RIPPLE is an improved implementation of the Continuum Surface Force (CSF) model (Brackbill et al., 1992) for evaluating surface tension effects. Rather than impose equation (3) as a discrete boundary condition for pressure at the free surface, the CSF model considers the interface to be continuous, and accounts for surface tension via an equivalent body force on fluid near the free surface. Unfortunately, the original RIPPLE contained an early implementation of the CSF model. One characteristic of this implementation was a tendency to induce spurious fluid motion in near-equilibrium surfaces (Brackbill et al., 1992). In fact, the authors employed the original RIPPLE in an early attempt to model the normal impact of a water droplet onto a flat surface. The CSF model induced very pronounced oscillations of the fluid, which became most apparent as the simulated droplet vainly attempted to reach some equilibrium configuration.

We have implemented several modifications to the original CSF model, inspired by recent suggestions by Kothe et al. (1996). We present here a short overview of our approach.

Surface tension forces $\vec{F}_{ST}$ are evaluated only in control volumes containing a portion of the free surface:

$$\vec{F}_{ST} = \sigma\kappa \frac{A}{V}\hat{n} \tag{5}$$

A is the free surface area contained within the control volume, determined as a by-product of the VOF advection algorithm of Youngs (1984). V is the volume of the control volume and $\hat{n}$ is a control volume-centred unit normal directed into the fluid. An accurate estimation of $\vec{F}_{ST}$ depends primarily on the evaluation of accurate normals, since the curvature κ is evaluated as:

$$\kappa = -\vec{\nabla} \cdot \hat{n} \tag{6}$$

Normal vectors $\vec{n}$ are first evaluated at control volume vertices, according to:

$$\vec{n} = \vec{\nabla} F \tag{7}$$

In practice, evaluating gradients of F can result in poor estimations of the normals. One alternative is to first smooth, or convolve, the F field (Brackbill et al., 1992). We employ a radially-symmetric cosine function as the convolving kernel $\delta_h(\vec{r})$ to smooth to a radius of $2h$:

$$\delta_h(\vec{r}) = \frac{3\pi}{32h^3(\pi^2-6)}\left\{1+\cos\left(\frac{\pi|\vec{r}|}{2h}\right)\right\}; \quad |\vec{r}| \le 2h$$
$$= 0; \quad |\vec{r}| > 2h \tag{8}$$

Aleinov and Puckett (1995) pointed out recently that in order to achieve convergence of $\vec{n}$ to a true value, that the radius over which to smooth must be related to grid size Δx by:

$$h \sim (\Delta x)^q; \qquad 0 < q < 1 \tag{9}$$

In other words, as the grid is refined, smoothing must occur over larger and larger stencils. For the two simulations presented in this paper, smoothing was performed over a 5x5x5 stencil. A control volume-centred unit normal $\hat{n}$ is then evaluated as the normalized average of the eight $\vec{n}$ at the vertices of the control volume. This tends to yield more accurate values of the normal $\hat{n}$ than averaging unit normals.

To evaluate κ, we locate the centre of the interface within the control volume, again as a by-product of the VOF advection algorithm of Youngs (1984). A more accurate κ is then calculated at this location than at the centre of the control volume. Like the calculation of the control volume-centred normal, this is another example of biasing calculations towards the true interface, where the magnitude of the normals is greatest.

Finally, we obtain better results if we slightly smooth the $\vec{F}_{ST}$. Like Aleinov and Puckett (1995), we simply employ the same smoothing kernel as for the F field, except that smoothing is contained within a smaller radius, limited to a 3x3x3 stencil.

RESULTS AND DISCUSSION

We present the results of two simulations, of a water droplet of 2 mm diameter, impacting a surface at 1 m/s. Both simulations were run on a square grid, with a control volume length equal to 1/20 of the initial droplet diameter.

Figure 1 illustrates photographs and numerical views of the impact of a water droplet onto a 45° incline. From the complete set of photographs, we measured advancing and receding contact angles (at the leading and trailing edges respectively). This data is presented in Figure 2. The contact angles were then imposed as a dynamic boundary condition on the simulation. Contact angles about the perimeter of the droplet were arbitrarily defined to vary linearly between the advancing and receding angles, according to the longitudinal position on the contact line.

The photographs and numerical views compare reasonably well, especially at early times. Initially fluid spreads almost uniformly about the point of impact ($t = 1$ ms). A large value of the contact angle at the top of the droplet reflects an advancing contact line. The photograph at $t = 1$ ms shows a droplet which is nearly symmetric, and almost identical to a corresponding droplet impacting normal to a flat surface. Quickly, however, the momentum of the droplet and the force of gravity begin to pull fluid down the incline. By $t = 2$ ms, the value of the contact angle at the top of the droplet is decreasing quickly, as the contact line begins to recede. Nonetheless, the droplet has spread enough in all directions that a ring of fluid has formed about the perimeter. At the centre of the droplet, the last of the falling fluid is still visible above the outer ring.

At $t = 5$ ms, the bulk of the fluid is collecting at the bottom of the splat, and the fluid is slowing, having flowed a considerable distance down the incline. Only a thin wedge of fluid remains above. Although it is difficult to see from the views in Figure 1, the splat is still a ring, with fluid on the periphery of the splat rather than at the centre. The view at $t = 8$ ms is of a droplet which has nearly stopped flowing down the incline. Only the thin wedge of fluid at the top of the splat is still moving downward. Surface tension now dominates, working against the mass of fluid at the bottom of the splat. By $t = 14$ ms, the wedge at the top has nearly rejoined the main body of fluid, and the droplet is approaching an equilibrium shape. This is an example of a photograph from which a receding contact angle measurement is difficult to obtain, as the wedge of fluid thins. By $t = 20$ ms, the droplet is still and at equilibrium.

Figure 3 presents the droplet spread factor, defined as the ratio of instantaneous liquid-solid contact diameter to initial droplet diameter. The plot demonstrates excellent agreement between experimental results and the numerical prediction,

especially in view of our arbitrary contact angle specification about the perimeter of the droplet.

Figure 4 illustrates photographs and numerical views of the impact of a 2 mm water droplet onto a sharp edge. We masked much of the cross-section of the surface when printing the photographs in order to highlight the edge itself. We arbitrarily selected the edge height to be one half of the droplet diameter. We also shifted the point of impact by 0.3 mm towards the top side of the edge, only because we wished to model the breakup of the droplet. We did experiment with a droplet centred exactly on the edge, but discovered that all of the fluid was consistently pulled to the bottom side. With regard to the contact angle boundary condition, we did not measure experimental contact angles from photographs. Instead, we used an approach similar to that of Fukai et. al. (1995). We simply defined an advancing contact angle to be 110°, a receding angle to be 40°, and interpolated linearly between these angles for contact line velocities less than ± 0.05 m/s.

We illustrate several profiles of the droplet during the early stages of deformation, as the droplet spreads over the top side and flows over the edge. Admittedly, at $t = 1.4$ ms, the simulation is unable to predict the gap between the edge and the fluid, likely due to the coarseness of the mesh. For the same reason, the simulation is unable to articulate subtle variations of the fluid surface. These details notwithstanding, agreement between experiment and simulation is very good. By $t = 2$ ms, droplet spread has generated a ring of fluid on the top side about the point of impact. By $t = 4$ ms, a similar ring has formed on the bottom side, and the edge itself has begun to separate fluid on top from fluid on the bottom. By $t = 8$ ms, the droplet has broken into two, and all that remains is for the droplet to reach an equilibrium position, illustrated at $t = 16$ ms.

CONCLUSIONS

We have presented a 3D numerical model to simulate the impact of droplets onto arbitrary surface geometries.

We also presented the results of two simulations, of the impact of a water droplet onto a 45° incline and onto an edge. Simulation results are compared with corresponding photographs taken of actual droplet impacts. Agreement is very good. Both the experimental and numerical results demonstrate complex, asymmetric flows, very different from the impact of a droplet normal to a flat surface.

REFERENCES

Aleinov, I. and Puckett, E.G., 1995, "Computing Surface Tension with High-Order Kernels," Proceedings of the 6th International Symposium on Computational Fluid Dynamics, K. Oshima, ed..

Brackbill, J.U., Kothe, D.B. and Zemach, C., 1992, "A Continuum Method for Modeling Surface Tension," Journal of Computational Physics, Vol. 100, 335-354.

Chandra, S. and Avedisian, C.T., 1991, "On the collision of a droplet with a solid surface," Proceedings of the Royal Society of London A, Vol. 432, pp. 13-41.

Fukai, J., Shiiba, Y., Yamamoto, T., Miyatake, O., Poulikakos, D., Megaridis, C.M. and Zhao, Z., 1995, "Wetting effects on the spreading of a liquid droplet colliding with a flat surface: Experiment and modeling," Physics of Fluids, Vol. 7, pp. 236-247.

Hirt, C.W. and Nichols, B.D., 1981, "Volume of Fluid (VOF) Method for the Dynamics of Free Boundaries," Journal of Computational Physics, Vol. 39, pp. 201-225.

Kothe, D.B., Mjolsness, R.C. and Torrey, M.D., 1991, "RIPPLE: A Computer Program for Incompressible Flows with Free Surfaces," Technical Report LA-12007-MS, LANL.

Kothe, D.B., Rider, W.J., Mosso, S.J., Brock, J.S. and Hochstein, J.I., 1996, "Volume Tracking of Interfaces Having Surface Tension in Two and Three Dimensions," Technical Report AIAA 96-0859.

Pasandideh-Fard, M., Qiao, Y.M., Chandra, S. and Mostaghimi, J., 1996, "Capillary effects during droplet impact on a solid surface," Physics of Fluids, Vol. 8, pp. 650-659.

Trapaga, G., Matthys, E.F., Valencia, J.J. and Szekely, J., 1992, "Fluid Flow, Heat Transfer, and Solidification of Molten Metal Droplets Impinging on Substrates: Comparison of Numerical and Experimental Results," Metallurgical Transactions B, Vol. 23B, pp. 701-718.

Youngs, D.L., 1984, "An Interface Tracking Method for a 3D Eulerian Hydrodynamics Code," Technical Report 44/92/35, AWRE.

Zhao, Z., Poulikakos, D. and Fukai, J., 1996a, "Heat transfer and fluid dynamics during the collision of a liquid droplet on a substrate - I. Modeling," International Journal of Heat and Mass Transfer, Vol. 39, pp. 2771-2789.

Zhao, Z., Poulikakos, D. and Fukai, J.,1996b, "Heat transfer and fluid dynamics during the collision of a liquid droplet on a substrate - II. Experiments," International Journal of Heat and Mass Transfer, Vol. 39, pp. 2791-2802.

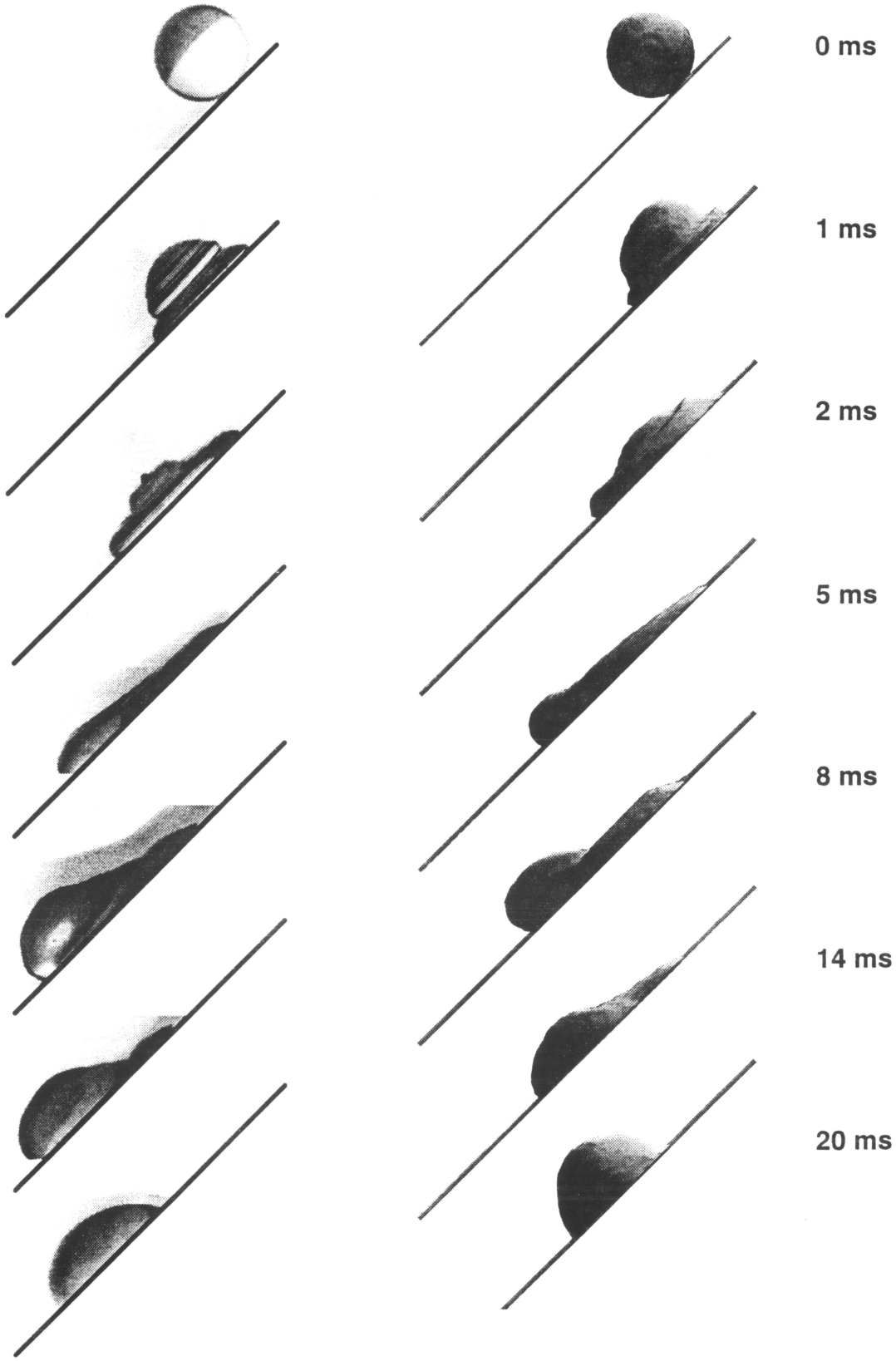

FIGURE 1. Impact of a water droplet onto a 45º incline - experimental and numerical views. [initial droplet diameter = 2 mm; initial droplet velocity = 1 m/s]

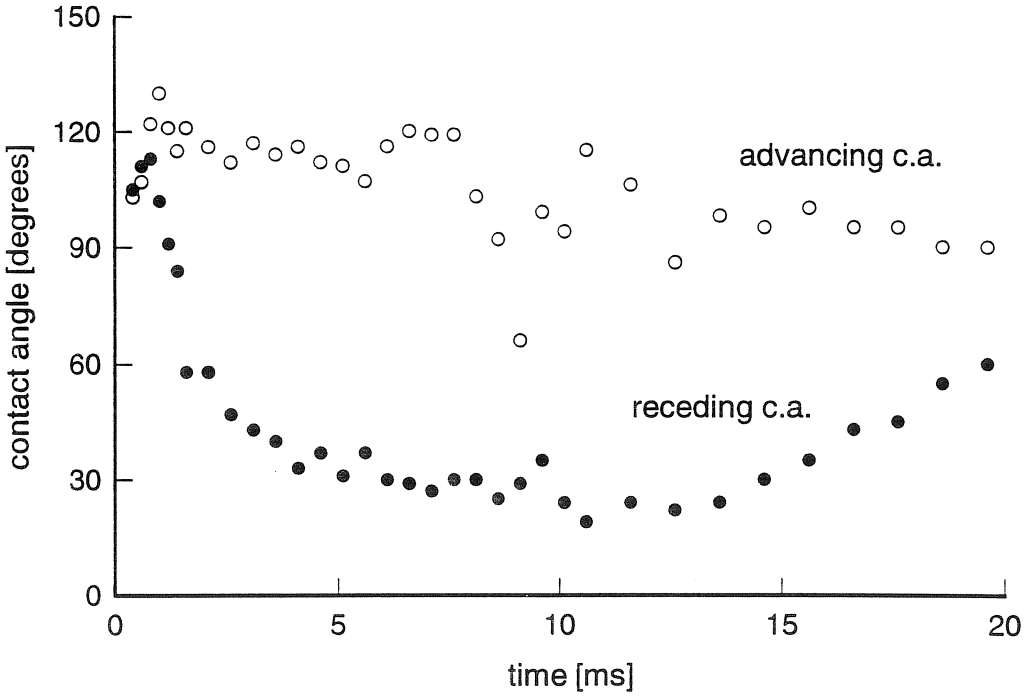

FIGURE 2. Advancing and receding contact angles - water droplet impact onto a 45º incline.

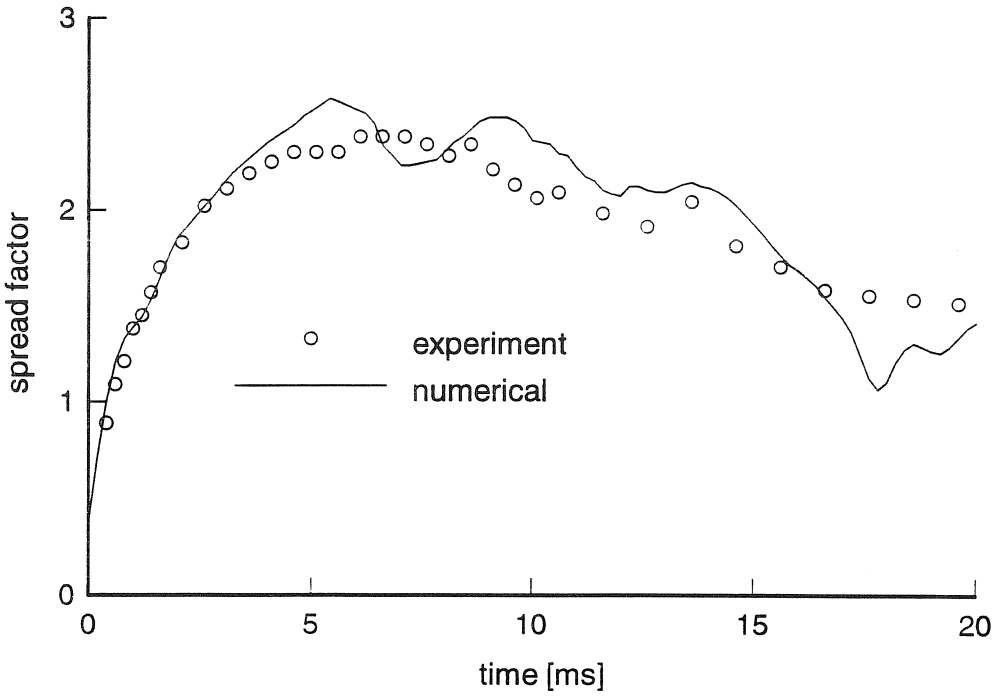

FIGURE 3. Spread factor (instantaneous diameter / initial droplet diameter) - water droplet impact onto a 45º incline.

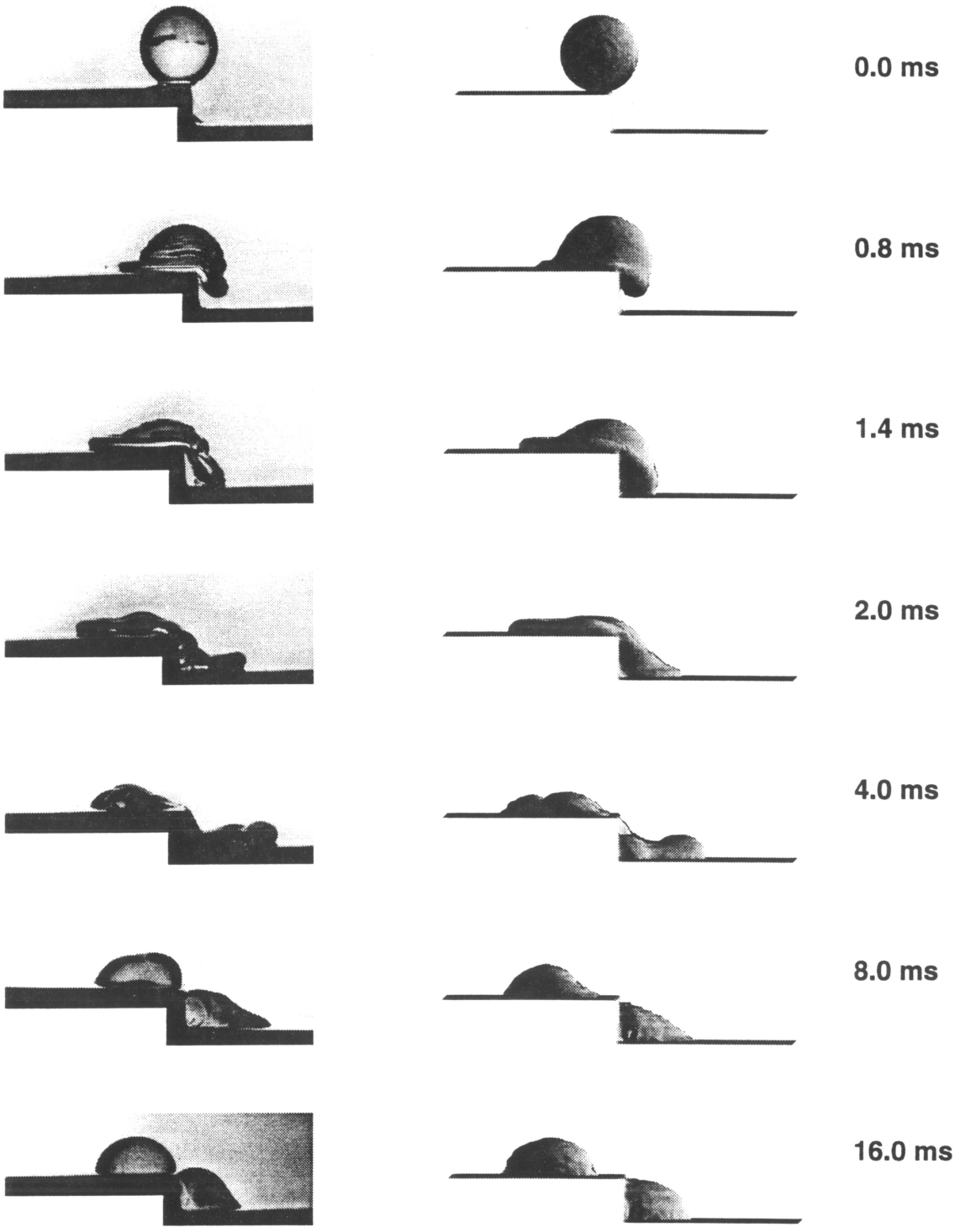

FIGURE 4. Impact of a water droplet onto an edge - experimental and numerical views. [initial droplet diameter = 2 mm; initial droplet velocity = 1 m/s; edge height = 1 mm]